

## On methods for stabilizing constraints over enriched interfaces in elasticity

Jessica D. Sanders, John E. Dolbow and Tod A. Laursen<sup>\*,†</sup>

*Duke Computational Mechanics Laboratory, Pratt School of Engineering,  
Duke University, Durham, NC 27708, U.S.A.*

### SUMMARY

Enriched finite element approaches such as the extended finite element method provide a framework for constructing approximations to solutions of non-smooth problems. Internal features, such as boundaries, are represented in such methods by using discontinuous enrichment of the standard finite element basis. Within such frameworks, however, imposition of interface constraints and/or constitutive relations can cause unexpected difficulties, depending upon how relevant fields are interpolated on un-gridded interfaces. This work address the stabilized treatment of constraints in an enriched finite element context.

Both the Lagrange multiplier and penalty enforcement of tied constraints for an arbitrary boundary represented in an enriched finite element context can lead to instabilities and artificial oscillations in the traction fields. We demonstrate two alternative variational methods that can be used to enforce the constraints in a stable manner. In a ‘bubble-stabilized approach,’ fine-scale degrees of freedom are added over elements supporting the interface. The variational form can be shown to have a similar form to a second approach we consider, Nitsche’s method, with the exception that the stabilization terms follow directly from the bubble functions.

In this work, we examine alternative variational methods for enforcing a tied constraint on an enriched interface in the context of two-dimensional elasticity. We examine several benchmark problems in elasticity, and show that only Nitsche’s method and the bubble-stabilization approach produce stable traction fields over internal boundaries. We also demonstrate a novel difference between the penalty method and Nitsche’s method in that the latter passes the patch test exactly, regardless of the stabilization parameter’s magnitude. Results for more complicated geometries and triple interface junctions are also presented. Copyright 2008 John Wiley & Sons, Ltd.

Received 17 June 2008; Revised 7 October 2008; Accepted 27 October 2008

KEY WORDS: X-FEM; stabilization; Nitsche’s method; constraints

---

\*Correspondence to: Tod A. Laursen, Duke Computational Mechanics Laboratory, Pratt School of Engineering, Duke University, Durham, NC 27708, U.S.A.

†E-mail: laursen@duke.edu

Contract/grant sponsor: Air Force Office of Scientific Research Grant; contract/grant number: FA9550-06-1-0108  
Contract/grant sponsor: Department of Defense National Defense Science and Engineering Fellowship Program  
Contract/grant sponsor: Department of Energy  
Contract/grant sponsor: Sandia National Laboratories

## 1. INTRODUCTION

Enriched finite element methods, including the extended finite element method (X-FEM) [1] and the generalized finite element method [2] use discontinuous enrichment of a finite element basis to capture inherently discontinuous physical behavior. These methods greatly enhance the kinematics of standard finite elements, and allow for the representation of discontinuities on interfaces that are independent of the mesh or ‘un-gridded’ (see [3], or Figure 1 for a schematic). Unfortunately, the enrichment also complicates the imposition of even simple constraints on these same surfaces, to the point where standard methods employing Lagrange multipliers or penalty regularization often trigger oscillations in the interfacial traction. In this work, we examine two alternatives, Nitsche’s method and a ‘bubble-stabilized’ approach, that stabilize the application of constraints for elasticity. To our knowledge, neither Nitsche’s method nor the bubble-stabilization approach has been applied to the problem of constraints imposed over enriched interfaces in elasticity.

The question of stable interface tractions is especially compelling in the context of granular interfaces, which necessarily involve some constraint on the inter-granular separation of material. The objective is to be able to represent the elastic response of a system of grains (with different material properties) separated by grain boundaries, without explicitly meshing the latter (Figure 1). To model the interfacial response, it may be of interest to use a cohesive model, a traction separation law, or even a model in which grains completely separate under a large enough load. To utilize an interfacial model, it is necessary to be able to accurately resolve the tractions over the enriched interface. A small amount of literature has addressed the problem of applying constraints to bodies across interfaces in enriched finite element methods [3–7].

The challenge of enforcing constraints across an internal discontinuity produced by an enriched solution field has some similarities to the numerics of other problems, including enforcing Dirichlet constraints on an enriched field and enforcing continuity constraints in meshfree, discontinuous enrichment methods [8] and discontinuous Galerkin [9–11] methods. The difficulty of enforcing

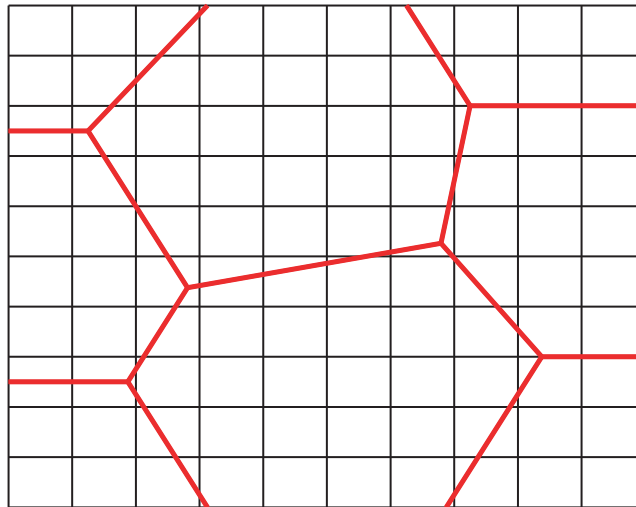


Figure 1. Example of un-gridded interfaces superimposed over a background mesh.

Dirichlet boundary conditions for enriched finite element and meshfree methods stems from the same issue, namely the construction of test functions that vanish over the Dirichlet boundary. The standard finite element approach of approximating the Dirichlet condition using only those nodes on the boundary is simply not an option when the boundary does not align with the mesh. As a result, recent attention has focused on methods that seek to enforce such constraints weakly.

Nitsche's method [12] was originally proposed as a method for weakly imposing essential boundary conditions for the finite element approximation of elliptical PDEs. The relationship to stabilized finite element methods was later established by Stenberg [13], who showed that Nitsche's method could be derived from the stabilized Lagrange multiplier formulation of Barbosa and Hughes [14]. The method has witnessed a resurgence in recent years, with applications ranging from boundary conditions in meshfree methods [15, 16] to constraints between overlapping finite element meshes [17]. Gracie *et al.* [9] have recently studied the application of Nitsche's method to internal boundaries modeled through a mixed X-FEM and discontinuous Galerkin method.

The problem of enforcing Dirichlet constraints for the X-FEM was examined by Ji and Dolbow [7], who showed that the most convenient choice of Lagrange multipliers triggered severe oscillations in the flux field. Penalty methods exhibit similar trends, with oscillations increasing as the penalty number increases and approaching the behavior of the unstable Lagrange multiplier formulation in a limiting sense. Moës *et al.* [5] subsequently developed a stable Lagrange multiplier method based on reducing the number of constraints on the interface. This approach has since been extended to contact conditions [6].

Another approach is to stabilize the convenient choice of Lagrange multipliers, as examined by Mourad *et al.* [18] in the context of enforcing Dirichlet conditions on arbitrary interfaces with the Laplace equation. Starting with the unstable Lagrange multiplier enforcement of Dirichlet constraints, the authors added bubble degrees of freedom to the enriched elements over which the constraints acted. Static condensation of the extra degrees of freedom yielded a weak formulation of the constraints nearly equivalent to Nitsche's method. The main difference is an expression for the stabilization parameter  $\alpha$  that follows directly from the mesh, interface geometry, and choice of bubble functions. In this work we extend this 'bubble-stabilization' technique to adherence constraints to be enforced between linearly elastic domains. Though the technique is rooted in the ideas of the variational multi-scale method [19], it has not previously been applied to this problem of enriched interfaces.

In this work, we compare four different techniques for applying constraints to interfaces that are enriched, and thus may exist on element interiors. Each technique represents a different variational form for the same set of governing equations. For simplicity of implementation, we consider the case in which perfect adherence conditions are enforced between bodies on either side of an interface. This 'tied problem' yields insight into the numerics and the various advantages and disadvantages of each technique. The work is therefore seen to represent an important first step toward the consideration of more complicated interface physics, such as cohesive laws.

Section 2 of the paper gives a general problem description for a two-dimensional elasticity problem with two grains, one internal boundary and a tied constraint. In Section 3 we present the four variational forms for the treatment of the interface, with some discussion of the development of the bubble-stabilized method. Section 4 discusses discretization of the problem including the enriched formulation. We briefly discuss the generalization of the methods to triple junctions and multiple grains in Section 5. Section 6 gives numerical results for several test problems with

and without internal interfaces, including beam bending, a thick walled pressure vessel, and a demonstrative multiple grain problem. Concluding remarks are given in Section 7.

## 2. PROBLEM DESCRIPTION AND GOVERNING EQUATIONS

A two-dimensional domain for a multi-grain elasticity boundary value problem is shown in Figure 2. The domain is comprised of two grains, open sets  $G_1$  and  $G_2$ , which share an internal boundary,  $\Gamma_*$ . The problem is posed as two grains, with the possibility of different material properties in each, and one interface. Problems consisting of multiple grains and interfaces may be treated by looping over interfaces, each only dividing two grains. Implementational details of dealing with triple junctions are given in Section 5.

The boundary of each grain can potentially be divided into three separate regions (Figure 3).  $\Gamma_*$  is the part of a grain boundary internal to  $\Omega$  and dividing two grains. It is shared by the grains on either side. The normal vector,  $n^{(m)}$ , will be defined as positive outwards from grain  $m$ . Any part of the grain boundary that is also an external boundary to  $\Omega$  will be classified according to the type of boundary condition applied at that point, either Dirichlet ( $\Gamma_d$ ) or Neumann ( $\Gamma_h$ ). Accordingly, we define:

$$\Omega = G^{(1)} \cup G^{(2)} \quad (1)$$

$$\Gamma^{(1)} = \Gamma_h^{(1)} \cup \Gamma_d^{(1)} \cup \Gamma_* \quad \text{and} \quad \Gamma^{(2)} = \Gamma_h^{(2)} \cup \Gamma_d^{(2)} \cup \Gamma_* \quad (2)$$

$$\Gamma_h = \Gamma_h^{(1)} \cup \Gamma_h^{(2)} \quad \text{and} \quad \Gamma_d = \Gamma_d^{(1)} \cup \Gamma_d^{(2)} \quad (3)$$

$$\Gamma = \Gamma_h \cup \Gamma_d \quad (4)$$

$$\Gamma_* = \cup \Gamma_e \quad (5)$$

$$\Gamma^{(m)} = \Gamma_h^{(m)} \cup \Gamma_d^{(m)} \cup \Gamma_* \quad (6)$$

It is worth remarking that the internal interface  $\Gamma_*$  is conceived as the union of subsegments  $\Gamma_e$ , which will notationally facilitate the development of numerical formulations once discretization is introduced. We leave the details of these subsegment definitions unspecified at the moment, while remarking that their definition in the discrete setting plays a crucial role in the stability properties of any numerical method.

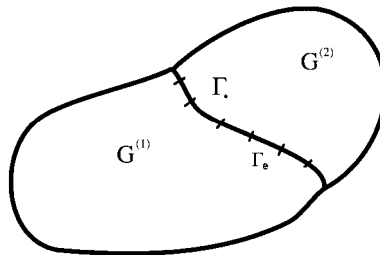


Figure 2. Problem domain for multi-grain elasticity.

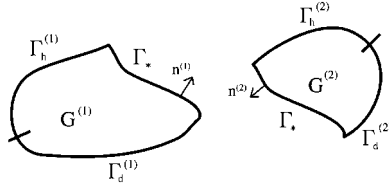


Figure 3. The problem domain decomposed into relevant pieces.

Using the above, we present governing equations for a small strain, elastic boundary value problem with a perfect bond at the interface. We follow the conventions of indicial notation, in which a repeated spatial index implies a sum. The strong form is given by

$$\sigma_{ij,j}^{(m)} = 0 \quad \text{in } G^{(m)}, \quad m = 1, 2 \quad (7)$$

$$u_i^{(m)} = g_i^{(m)} \quad \text{on } \Gamma_d^{(m)}, \quad m = 1, 2 \quad (8)$$

$$\sigma_{ij}^{(m)} n_j^{(m)} = h_i^{(m)} \quad \text{on } \Gamma_h^{(m)}, \quad m = 1, 2 \quad (9)$$

$$u_i^{(1)} = u_i^{(2)} \quad \text{on } \Gamma_* \quad (10)$$

$$\sigma_{ij}^{(1)} n_j^{(1)} = -\sigma_{ij}^{(2)} n_j^{(2)} \quad \text{on } \Gamma_* \quad (11)$$

where

$$\sigma_{ij}^{(m)} = C_{ijkl}^{(m)} u_{(k,l)}^{(m)}, \quad m = 1, 2 \quad (12)$$

The primary unknown is the displacement,  $u_i$ , over  $\Omega$ , which can be seen as the collection of the displacement fields over each grain,  $u_i^{(1)}$  and  $u_i^{(2)}$ .

The enriched finite element method [1, 2, 20] for our problem departs from the traditional method in the assumed form of the displacement field over the body. In particular, we assume that the displacement field can be decomposed into continuous and discontinuous parts, with the latter contributing only in the vicinity of the interface. The addition of a discontinuous function near the interface geometry allows the kinematics to properly capture the form of the solution at the interface. Near the interface, the enriched displacement field is given by

$$u_i(\mathbf{x}) = \hat{u}_i(\mathbf{x}) + \sum_m H(\mathbf{x})^{(m)} \tilde{u}_i^{(m)}(\mathbf{x}) \in S \quad (13)$$

with the variation taking the same form:

$$w_i(\mathbf{x}) = \hat{w}_i(\mathbf{x}) + \sum_m H(\mathbf{x})^{(m)} \tilde{w}_i^{(m)}(\mathbf{x}) \in V \quad (14)$$

where the spaces of the displacements  $S$  and the variations  $V$  are defined as

$$S = \{u_i(\mathbf{x}) | u_i(\mathbf{x}) \in H^1, u_i(\mathbf{x}) = g_i \text{ on } \Gamma_d, u_i(\mathbf{x}) \text{ discontinuous on } \Gamma_*\} \quad (15)$$

$$V = \{w_i(\mathbf{x}) | w_i(\mathbf{x}) \in H^1, w_i(\mathbf{x}) = 0 \text{ on } \Gamma_d, w_i(\mathbf{x}) \text{ discontinuous on } \Gamma_*\} \quad (16)$$

With such a decomposition,  $\hat{u}_i$  can be seen as a coarse-scale field, which is active over the entire domain and  $\tilde{u}_i^{(m)}$  is a local solution that is restricted to an individual grain  $m$  through multiplication by a characteristic grain function  $H(\mathbf{x})^{(m)}$ . The function  $H(\mathbf{x})^{(m)}$  is equal to one over the domain of grain  $m$  and zero everywhere else, i.e.

$$H(\mathbf{x})^{(m)} = \begin{cases} 1 & \text{if } \mathbf{x} \in G^{(m)} \\ 0 & \text{otherwise} \end{cases} \quad (17)$$

Individually, both  $\hat{u}_i$  and  $\tilde{u}_i$  belong to the smooth space of all  $H^1(\Omega)$  continuous functions. For convenience we will use the shorthand notations  $H^{(m)}$  to indicate  $H(\mathbf{x})^{(m)}$  and  $w_i$  and  $u_i$  to indicate  $w_i(\mathbf{x})$  and  $u_i(\mathbf{x})$ , respectively.

### 3. VARIATIONAL FORM

To begin, we present the variational form of the enriched finite element method for an untied problem. Later, we will constrain the kinematics across the internal interface by adding terms to the variational form according to the particular method (e.g. Lagrange multiplier, Nitsche, etc.) of interest. In the internally traction-free (untied) problem, Equations (10) and (11) are replaced with

$$\sigma_{ij}^{(1)} n_j^{(1)} = \sigma_{ij}^{(2)} n_j^{(2)} = 0 \quad \text{on } \Gamma_* \quad (18)$$

Now, upon multiplying (7) by a weighting function, integrating by parts, applying Gauss' theorem, and including the boundary conditions, the following problem is obtained: Find  $\mathbf{u} \in \mathcal{S}$  such that

$$\begin{aligned} & \int_{\Omega} \hat{w}_{i,j} \sigma_{ij} \, d\Omega + \sum_m \int_{G^{(m)}} \tilde{w}_{i,j}^{(m)} \sigma_{ij}^{(m)} \, dG^{(m)} \\ & = \int_{\Gamma_h} \hat{w}_i h_i \, d\Gamma_h + \sum_m \int_{\Gamma_h^{(m)}} \tilde{w}_i^{(m)} h_i^{(m)} \, d\Gamma_h^{(m)} \quad \text{for all } \mathbf{w} \in V \end{aligned} \quad (19)$$

where  $m$  is the global grain numbering index as discussed before.

We now examine various methods for weakly enforcing the interfacial conditions (10) and (11). As the jump in the displacement field over  $\Gamma_*$  will appear in the variational form for each method, we introduce a shorthand notation for it via  $[[u_i]] = (u_i^{(1)} - u_i^{(2)})$ . This can be written equivalently as  $[[u_i]] = (\tilde{u}_i^{(1)} - \tilde{u}_i^{(2)})$ , since the background field is assumed to be continuous at the interface.

#### 3.1. Lagrange multipliers

To develop the Lagrange multiplier method, we start with the variational form representing the boundary value problem with no tractions over  $\Gamma_*$  (as summarized in (19)), and then assume a traction field, belonging to the space  $L$ , represented by  $\lambda$  acting over the interface  $\Gamma_*$ .

$$L = \{\lambda_i(\mathbf{x}) \mid \lambda_i(\mathbf{x}) \in L^2(\Gamma_*)\} \quad (20)$$

We introduce an additional equation corresponding to the tied condition (10). The Lagrange multiplier problem is: Find  $(\mathbf{u}, \boldsymbol{\lambda}) \in S \times L$  such that

$$\begin{aligned} & \int_{\Omega} \hat{w}_{i,j} \sigma_{ij} \, d\Omega + \sum_m \int_{G^{(m)}} \tilde{w}_{i,j}^{(m)} \sigma_{ij}^{(m)} \, dG^{(m)} + \int_{\Gamma_*} \lambda_i \llbracket w_i \rrbracket \, d\Gamma_* \\ & = \int_{\Gamma_h} \hat{w}_i h_i \, d\Gamma_h + \sum_m \int_{\Gamma_h^{(m)}} \tilde{w}_i^{(m)} h_i^{(m)} \, d\Gamma_h^{(m)} \\ & \int_{\Gamma_*} \mu_k \llbracket u_k \rrbracket \, d\Gamma_* = 0 \quad \text{for all } (\mathbf{w}, \boldsymbol{\mu}) \in V \times L \end{aligned} \quad (21)$$

One major disadvantage of mixed methods such as the Lagrange multiplier method is that when discretized, their performance is dependent on the finite element subspaces satisfying the so-called LBB (or inf-sup) conditions. For embedded interface methods, this rules out many convenient choices for the subspaces. This is discussed in Section 4.

### 3.2. Penalty method

The penalty method is a way of approximating the Lagrange multiplier problem. We approximate the multiplier field with

$$\lambda_i \approx \alpha \llbracket u_i \rrbracket \quad (22)$$

where  $\alpha$  is some large number that can be interpreted as a gap stiffness, and will be referred to as the penalty parameter. The constraint is only represented in the limit  $\alpha \rightarrow \infty$ .

The variational form for the penalty method is: Find  $\mathbf{u} \in S$  such that

$$\begin{aligned} & \int_{\Omega} \hat{w}_{(i,j)} \sigma_{ij} \, d\Omega + \sum_m \int_{G^{(m)}} \tilde{w}_{(i,j)}^{(m)} \sigma_{ij}^{(m)} \, dG^{(m)} + \alpha \int_{\Gamma_*} \llbracket u_i \rrbracket \llbracket w_i \rrbracket \, d\Gamma_* \\ & = \int_{\Gamma_h} \hat{w}_i h_i \, d\Gamma_h + \sum_m \int_{\Gamma_h^{(m)}} \tilde{w}_i^{(m)} h_i^{(m)} \, d\Gamma_h^{(m)} \quad \text{for all } \mathbf{w} \in V \end{aligned} \quad (23)$$

The advantage of the penalty method is that there are no additional global constraint equations and only one unknown (the displacement field). However, the penalty method can be shown to be variationally inconsistent, and discrete results can be overly sensitive to  $\alpha$ . A classic result by Babuška [21] indicates that for good convergence with mesh refinement, the penalty parameter must grow at a rate that outpaces the other terms in the stiffness matrix. For the discretized method, this eventually leads to poor conditioning of the linear algebraic system of equations.

### 3.3. Nitsche's method

A method for treatment of the tied constraint, in the form of Nitsche, can be expressed for the enriched elasticity problem as: Find  $\mathbf{u} \in S$  such that

$$\int_{\Omega} \hat{w}_{(i,j)} \sigma_{ij} \, d\Omega + \sum_m \int_{G^{(m)}} \tilde{w}_{(i,j)}^{(m)} \sigma_{ij}^{(m)} \, dG^{(m)} + \alpha \sum_{\Gamma_e} \int_{\Gamma_e} \llbracket u_i \rrbracket \, d\Gamma_e \int_{\Gamma_e} \llbracket w_i \rrbracket \, d\Gamma_e$$

$$\begin{aligned}
 & - \int_{\Gamma_*} \llbracket w_i \rrbracket \langle \sigma_{ij} \rangle n_j^{(1)} d\Gamma - \int_{\Gamma_*} \llbracket u_i \rrbracket \langle \sigma(w)_{ij} \rangle n_j^{(1)} \\
 & = \int_{\Gamma_h} \hat{w}_i h_i d\Gamma_h + \sum_m \int_{\Gamma_h^{(m)}} \tilde{w}_i^{(m)} h_i^{(m)} d\Gamma_h^{(m)} \quad \text{for all } \mathbf{w} \in V
 \end{aligned} \tag{24}$$

where

$$\langle a_{ij} \rangle = \frac{1}{2}(a_{ij}^{(1)} + a_{ij}^{(2)})$$

is an average operator on the interface.

An alternate form, often found in the literature, replaces  $\alpha \sum_{\Gamma_e} \int_{\Gamma_e} \llbracket u_i \rrbracket d\Gamma_e \int_{\Gamma_e} \llbracket w_i \rrbracket d\Gamma_e$  in (24) with  $\hat{\alpha} \int_{\Gamma_*} \llbracket u_i \rrbracket \llbracket w_i \rrbracket d\Gamma_*$ . We note the difference in dimensionality between these two forms: the stabilization parameter  $\alpha$  is expected to scale in proportion to  $1/h^2$ , while  $\hat{\alpha}$  should scale as  $1/h$ , where  $h$  is a measure of mesh size.

As in the penalty method,  $\alpha$  is a free parameter for Nitsche's method. Rather than a penalty parameter, however, it is more properly viewed as a stabilization parameter in the context of this method. As such, it is expected to be relatively 'small', but it should be noted that for arbitrary values of  $\alpha$  there is no guarantee that the bilinear form will remain positive definite. It has been shown [15] that a minimum  $\alpha$  exists that will guarantee positive definiteness of the bilinear form associated with Nitsche's method.

#### 4. DISCRETIZATION

We partition the domain into a set of elements independently of the geometry of any internal interface; hence, elements may be seen to be 'cut' by  $\Gamma_*$  (Figure 1). In the near field of the interface, defined as anywhere a nodal support intersects the interface, the enriched approximation of the solution and its variation over an element take the form

$$u_i^h(\mathbf{x}) = \sum_a N_a(\mathbf{x}) \hat{d}_{ai} + \sum_m \sum_e H^{(m)} N_e^{(m)}(\mathbf{x}) \tilde{d}_{ei} \tag{25}$$

$$w_i^h(\mathbf{x}) = \sum_b N_b(\mathbf{x}) \hat{c}_{bi} + \sum_m \sum_f H^{(m)} N_f^{(m)}(\mathbf{x}) \tilde{c}_{fi} \tag{26}$$

where  $N_a, N_e, N_b$ , and  $N_f$  are standard finite element shape functions, and may be any of various shape functions traditionally used. In this work, we use piecewise-linear functions over three-node triangular elements. Lower case, roman indices  $a, b, e$ , and  $f$  represent local indices for the three nodes associated with each element.

Any node that has an approximate solution field that includes an additional local degree of freedom multiplied by a characteristic function  $H^{(m)}$  will be referred to as an enriched element. An important aspect of the method is that enrichment is only necessary for nodes with supports that are crossed by an interface. Sufficiently far from an interface, a standard interpolation is used. Many References [1, 2, 22] give the discrete form of the bulk stiffness terms for elements with discontinuous enrichment that assemble to form a global stiffness matrix  $\mathbf{K}$  that gives rise to the system  $\mathbf{Kd} = \mathbf{F}$ .

4.1. Lagrange multipliers

To implement Lagrange multipliers we must make a choice for the interpolation of the multipliers over the interface. In this study, the Lagrange multipliers are assumed to be piecewise constant over each  $\Gamma_e$ . The choice of a piecewise constant subspace is convenient and easy to implement, but is shown to have stability problems. Recent work by Moës *et al.* [5, 6] demonstrates that careful construction of the multiplier space can circumvent the stability problems introduced by a naive choice of multipliers; here, by contrast, we consider precisely such a naive (but easy to implement) choice and investigate how oscillations may be stabilized.

The discretization of the Lagrange multipliers is achieved via

$$\lambda_i = \sum_l \hat{N}_l \lambda_{li} \tag{27}$$

where  $\hat{N}_l$  is a Lagrange multiplier shape function equal to 1 over the segment  $l$  and 0 over all other segments, and  $l$  is an index over the segments  $\Gamma_e$ .

The final discrete form of the equations is

$$\begin{bmatrix} \mathbf{K} & \mathbf{G}^T \\ \mathbf{G} & \mathbf{0} \end{bmatrix} \begin{bmatrix} \mathbf{d} \\ \boldsymbol{\lambda} \end{bmatrix} = \begin{bmatrix} \mathbf{F} \\ \mathbf{0} \end{bmatrix} \tag{28}$$

where  $\mathbf{K}$  is the stiffness matrix arising from the standard (enriched) finite element method,  $\mathbf{G}$  is a global matrix assembled from the discretization of the boundary terms,  $\mathbf{d}$  is the vector of unknown displacement degrees of freedom, and  $\boldsymbol{\lambda}$  is a vector of unknown Lagrange multipliers. For a two-dimensional, three-node element with enrichment at every node, there will be 12 degrees of freedom, meaning that the element stiffness matrix will be  $12 \times 12$  (see Figure 4). The term  $\mathbf{G}$  is assembled from  $2 \times 12$  local contributions  $\mathbf{g}$  of individual elements containing segments  $\Gamma_e$ , which are

$$\mathbf{g} = [\mathbf{0}_{2 \times 6} | \mathbf{g}^{e,l}] \tag{29}$$

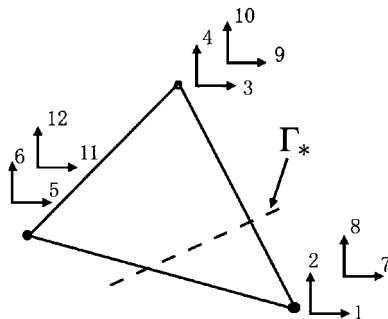


Figure 4. Example node numbering scheme for an enriched element. The classical degrees of freedom comprise numbers 1–6, while the enriched degrees of freedom comprise numbers 7–12. Horizontal and vertical arrows denote  $x$  and  $y$  components of the displacement field, respectively.

where  $\mathbf{g}^{e,l}$  comes from the constraints that act directly on the enriched degrees of freedom of the element:

$$\mathbf{g}^{e,l} = \int_{\Gamma_e} \hat{\mathbf{N}}_l \mathbf{N}^e d\Gamma_e \quad (30)$$

The matrix  $\hat{\mathbf{N}}_l$  contains the Lagrange multiplier shape functions associated with interface segment  $l$ :

$$\hat{\mathbf{N}}_l = \begin{bmatrix} \hat{N}_l & 0 \\ 0 & \hat{N}_l \end{bmatrix} \quad (31)$$

while the matrix  $\mathbf{N}^e$  contains the local element shape functions:

$$\mathbf{N}^e = [\mathbf{N}_1^e \quad \mathbf{N}_2^e \quad \mathbf{N}_3^e] \quad (32)$$

and

$$\mathbf{N}_r^e = \begin{bmatrix} H^{(1)} N_r^{(1)} - H^{(2)} N_r^{(2)} & 0 \\ 0 & H^{(1)} N_r^{(1)} - H^{(2)} N_r^{(2)} \end{bmatrix}, \quad r = 1, 2, 3 \quad (33)$$

The non-zero contribution to  $\mathbf{g}$  comes from the enriched degrees of freedom via  $\mathbf{g}^{e,l}$ , which is  $2 \times 6$  in this case. The index over the rows of  $\mathbf{g}$  corresponds to equation numbers for the Lagrange multiplier degrees of freedom, with local index  $l$ . The index over the columns represents the element degrees of freedom.

#### 4.2. Penalty method

The discrete form of the penalty method is

$$(\mathbf{K} + \mathbf{K}^P) \mathbf{d} = \mathbf{F} \quad (34)$$

A global penalty stiffness  $\mathbf{K}^P$  is assembled from element matrices  $\mathbf{k}^P$ . Construction of the element stiffnesses is done from a discretization of the boundary terms in the following way:

$$\mathbf{k}^P = \left[ \begin{array}{c|c} \mathbf{0}_{6 \times 6} & \mathbf{0}_{6 \times 6} \\ \hline \mathbf{0}_{6 \times 6} & \mathbf{k}_e^P \end{array} \right] \quad (35)$$

For a two-dimensional, three-node element with enrichment at every node, (35) represents a  $12 \times 12$  local element matrix. Figure 4 shows a numbering scheme for the case in which each node has two standard degrees of freedom and two degrees of freedom representing the enrichment. The classical degrees of freedom comprise numbers 1–6, while the enriched degrees of freedom comprise numbers 7–12. The penalty term involves only enriched degrees of freedom, which is why (38) is mostly populated with 0s. The non-zero contribution comes from

$$\mathbf{k}_e^P = \alpha \int_{\Gamma_e} \mathbf{N}^{eT} \mathbf{N}^e d\Gamma_e \quad (36)$$

### 4.3. Nitsche's method

The discrete form of the equations in Nitsche's method is

$$[\mathbf{K} + \mathbf{K}^s + \mathbf{K}^n + (\mathbf{K}^n)^T] \mathbf{d} = \mathbf{F} \quad (37)$$

A global stabilization stiffness  $\mathbf{K}^s$  is constructed from element matrices  $\mathbf{k}^s$ , in a very similar way to the specification of the penalty contributions:

$$\mathbf{k}^s = \begin{bmatrix} \mathbf{0}_{6 \times 6} & \mathbf{0}_{6 \times 6} \\ \mathbf{0}_{6 \times 6} & \mathbf{k}_e^s \end{bmatrix} \quad (38)$$

where

$$\mathbf{k}_e^s = \alpha \int_{\Gamma_e} \mathbf{N}^{eT} d\Gamma_e \int_{\Gamma_e} \mathbf{N}^e d\Gamma_e \quad (39)$$

$\mathbf{K}^n$  is constructed from elemental matrices

$$\mathbf{k}^n = [k_{pq}^e] = \int_{\Gamma_e} (N_e^{(1)} - N_e^{(2)}) \frac{[C_{ijkl}^{(1)}(N_{b,l} + N_{f,l}^{(1)}) + C_{ijkl}^{(2)}(N_{b,l} + N_{f,l}^{(2)})] n_j^{(1)}}{2} \quad (40)$$

where

$$p = 2(e-1) + i \quad \text{and} \quad q = 2(f-1) + k \quad (41)$$

Nitsche's method can be derived by starting with the discrete Lagrange multiplier problem and substituting an element wise approximation of the multipliers as

$$\lambda_i^e = \alpha \sum_{\Gamma_e} \int_{\Gamma_e} [[\tilde{u}_i]] d\Gamma_e - \langle \sigma_{ij} \rangle^e n_j \quad (42)$$

For the alternate form of Nitsche's method, the contributions to the element stiffness matrix take the form of (38), with the modification

$$\mathbf{k}_e^s = \hat{\alpha} \int_{\Gamma_e} \mathbf{N}^{eT} \mathbf{N}^e d\Gamma_e \quad (43)$$

In this case we may solve a discrete problem to find an estimate of the parameter  $\hat{\alpha}$ . Having applied a discretization to the domain, we may impose a condition on the vector fields so that the bilinear form may be guaranteed to be positive definite.

We first introduce the energy norm and  $L^2$  norm of a vector field, which are, respectively,

$$\|\mathbf{w}\|_{E(\Omega)} = \sqrt{\int_{\Omega} w_{i,j} C_{ijkl} w_{k,l} d\Omega} \quad (44)$$

and

$$\|\mathbf{w}\|_{L_2(\Omega)} = \sqrt{\int_{\Omega} w_i w_i d\Omega} \quad (45)$$

With some substitution, we can introduce Nitsche's bilinear form as

$$\begin{aligned}
 a(\mathbf{w}, \mathbf{w}) &= \|\mathbf{w}^{(1)}\|_{E(G^{(1)})}^2 + \|\mathbf{w}^{(2)}\|_{E(G^{(2)})}^2 - \int_{\Gamma} \llbracket w_i \rrbracket C_{ijkl}^{(1)} w_{k,l}^{(1)} n_j^{(1)} d\Gamma \\
 &\quad - \int_{\Gamma} \llbracket w_i \rrbracket C_{ijkl}^{(2)} w_{k,l}^{(2)} n_j^{(1)} d\Gamma + \hat{\alpha} \|\llbracket \mathbf{w} \rrbracket\|_{L_2(\Gamma)}^2
 \end{aligned} \tag{46}$$

Applying the Cauchy Schwarz inequality and rearranging yields

$$\begin{aligned}
 a(\mathbf{w}, \mathbf{w}) &\geq \|\mathbf{w}^{(1)}\|_{E(G^{(1)})}^2 + \|\mathbf{w}^{(2)}\|_{E(G^{(2)})}^2 - \|\llbracket \mathbf{w} \rrbracket\|_{L_2(\Gamma)} (\|C_{ijkl}^{(1)} w_{k,l}^{(1)} n_j^{(1)}\|_{L_2(\Gamma)} \\
 &\quad + \|C_{ijkl}^{(2)} w_{k,l}^{(2)} n_j^{(1)}\|_{L_2(\Gamma)}) + \hat{\alpha} \|\llbracket \mathbf{w} \rrbracket\|_{L_2(\Gamma)}^2
 \end{aligned} \tag{47}$$

If we choose to impose the condition,<sup>‡</sup>

$$\|C_{ijkl}^{(1)} w_{k,l}^{(1)} n_j^{(1)}\|_{L_2(\Gamma)} + \|C_{ijkl}^{(2)} w_{k,l}^{(2)} n_j^{(1)}\|_{L_2(\Gamma)} \leq C_1 (\|\mathbf{w}^{(1)}\|_{E(G^{(1)})} + \|\mathbf{w}^{(2)}\|_{E(G^{(2)})}) \tag{48}$$

for some mesh-dependent  $C_1 > 0$ , we can substitute the right side of (48) in (47) and get, with some algebra and rearranging,

$$\begin{aligned}
 a(\mathbf{w}, \mathbf{w}) &\geq \|\mathbf{w}^{(1)}\|_{E(G^{(1)})}^2 - C_1 \|\llbracket \mathbf{w} \rrbracket\|_{L_2(\Gamma)} \|\mathbf{w}^{(1)}\|_{E(G^{(1)})} + \frac{\hat{\alpha}}{2} \|\llbracket \mathbf{w} \rrbracket\|_{L_2(\Gamma)}^2 \\
 &\quad + \|\mathbf{w}^{(2)}\|_{E(G^{(2)})}^2 - C_1 \|\llbracket \mathbf{w} \rrbracket\|_{L_2(\Gamma)} \|\mathbf{w}^{(2)}\|_{E(G^{(2)})} + \frac{\hat{\alpha}}{2} \|\llbracket \mathbf{w} \rrbracket\|_{L_2(\Gamma)}^2
 \end{aligned} \tag{49}$$

This can be manipulated to yield

$$a(\mathbf{w}, \mathbf{w}) \geq \frac{\|\mathbf{w}^{(1)}\|_{E(G^{(1)})}^2}{2} + \left(\frac{\hat{\alpha}}{2} - \frac{C_1^2}{2}\right) \|\llbracket \mathbf{w} \rrbracket\|_{L_2(\Gamma)}^2 + \frac{\|\mathbf{w}^{(2)}\|_{E(G^{(2)})}^2}{2} + \left(\frac{\hat{\alpha}}{2} - \frac{C_1^2}{2}\right) \|\llbracket \mathbf{w} \rrbracket\|_{L_2(\Gamma)}^2 \tag{50}$$

We can assure that  $a(\mathbf{w}, \mathbf{w})$  is positive definite if  $\hat{\alpha} > C_1^2$  subject to condition (48). This holds because all other quantities on the right side of (50) are positive definite.

Following the work of Griebel and Schweitzer [15], we propose solving an eigenvalue problem to estimate  $C_1$  for the discretized space, based on condition (48). The generalized eigenvalue problem reads

$$\mathbf{Ax} = \mathbf{Bx} \tag{51}$$

where  $\mathbf{\Lambda}$  are the eigenvalues. The maximum eigenvalue of (51) is a good estimate for  $C_1^2$ .

The construction of the matrices  $\mathbf{A}$  and  $\mathbf{B}$  is based on the approximations to the bulk field (Equations (25) and (26)) and the condition (48).  $\mathbf{A}$  and  $\mathbf{B}$  are assembled from element level matrices

$$[a_{pq}^e] = \sum_m \int_{\Gamma_e} (C_{ijkl}^{(m)} N_{f,l}^{(m)} n_j^{(1)}) (C_{iwyz}^{(m)} N_{g,z}^{(m)} n_w^{(1)}) d\Gamma_e \tag{52}$$

<sup>‡</sup>Strictly speaking, valid only in the discrete setting.

which is condensed via

$$p = 2(f - 1) + k \quad \text{and} \quad q = 2(g - 1) + y \quad (53)$$

and

$$\begin{aligned} [b_{pq}^e] = & \int_{\Omega} N_{a,j} C_{ijkl} N_{b,l} \, d\Omega + \sum_m \int_{G^{(m)}} N_{a,j} C_{ijkl}^{(m)} N_{f,l}^{(m)} \, dG^{(m)} \\ & + \sum_m \int_{G^{(m)}} N_{e,j}^{(m)} C_{ijkl}^{(m)} N_{b,l} \, dG^{(m)} + \sum_m \int_{G^{(m)}} N_{e,j}^{(m)} C_{ijkl}^{(m)} N_{f,l}^{(m)} \, dG^{(m)} \end{aligned} \quad (54)$$

which is condensed via

$$p = 2(a - 1) + i \quad \text{and} \quad q = 2(b - 1) + k \quad (55)$$

in the case of the shape function contribution for the standard degrees of freedom, or

$$p = 2(e - 1) + i \quad \text{and} \quad q = 2(f - 1) + k \quad (56)$$

in the case of enriched shape functions.

#### 4.4. Bubble-stabilized approach

Having a discretization in place allows us to propose a fourth method. The bubble-stabilized approach is based on an improvement of the Lagrange multiplier method, recognizing that in all likelihood a convenient choice of multiplier will not satisfy LBB stability conditions, and thus will result in oscillatory multipliers. The approach involves starting with a Lagrange multiplier form of the problem and adding additional fine-scale degrees of freedom to the displacement field. The extra degrees of freedom use basis functions that resemble bubbles over element domains and are only added over elements intersecting  $\Gamma_*$ . Adding extra degrees of freedom at the interface can have a stabilizing effect on the solution for the multipliers. Similar work has been done for the Laplace equation with one-sided Dirichlet constraints [18]. Through the static condensation of the additional degrees of freedom, a variational form can be developed that is nearly equivalent to Nitsche's method, with the free parameter  $\alpha$  replaced by a term that is a function of the choice of the bubble basis functions. The problem of choosing a stabilization parameter for Nitsche's method is replaced by the problem of choosing suitable bubble functions.

We begin by reconsidering the Lagrange multiplier form of the problem given in (21), under the condition of homogeneous traction boundary conditions (this assumption is made for simplicity only; it has no bearing on the steps of the argument). An important feature of the derivation is that the multiplier fields and the variations are assumed to be piecewise constant over each  $\Gamma_e$ . Under these conditions, the formulation can be rearranged to read

$$\sum_m \int_{G^{(m)}} w_{i,j}^{(m)} C_{ijkl}^{(m)} u_{k,l}^{(m)} \, dG^{(m)} + \int_{\Gamma_*} \lambda_i (w_i^{(1)} - w_i^{(2)}) \, d\Gamma_* = 0 \quad (57)$$

and

$$\int_{\Gamma_*} \mu_k (u_k^{(1)} - u_k^{(2)}) \, d\Gamma = 0 \quad (58)$$

Over elements split by the internal interface, suppose that both  $u_k$  and  $w_i$  are composed of coarse (indicated by an overbar) and fine scales,

$$u_k^e = \bar{u}_k^e + u_k'^e \quad \text{and} \quad w_i^e = \bar{w}_i^e + w_i'^e \quad (59)$$

where enrichment still occurs in the sense that

$$\bar{u}_k^e = \hat{u}_k^e + \sum_m H^{(m)} \tilde{u}_k^{(m),e} \quad (60)$$

We introduce the element level fine-scale approximations:

$$u_k'^{(m),e} = b^{(m),e} \beta_k^e \quad \text{and} \quad w_i'^{(m),e} = b^{(m),e} \gamma_i^e \quad (61)$$

where  $b$  is some bubble basis function defined over the element domain and  $b^{(m),e} = \sum_m H^{(m)} b^e$ .  $\beta_k^e$  are fine-scale degrees of freedom and  $\gamma_i^e$  are the associated variations. In order to introduce an element level function, as well as a shape function, it is noted that we are necessarily looking at a discretized system. In these studies, we implemented a bubble that is simply the product of the linear triangle shape functions for a given element.

$$b^e = N_1 N_2 N_3 \quad (62)$$

Going through the process of static condensation of the fine-scale degrees of freedom yields the following variational form:

Find  $\mathbf{u} \in S$  such that

$$\begin{aligned} & \sum_e \left[ \sum_{m^e} \int_{G^{(m^e)}} (\bar{w}_{i,j})^{(m^e),e} C_{ijkl}^{(m^e)} (\bar{u}_{k,l})^{(m^e),e} dG_e^{(m^e)} \right. \\ & - \langle \bar{\sigma}_{kl}(\bar{w}) \rangle^e n_l \int_{\Gamma_e} (\bar{u}_k^{(1),e} - \bar{u}_k^{(2),e}) d\Gamma_e - \langle \bar{\sigma}_{ij} \rangle^e n_j \int_{\Gamma_e} (\bar{w}_i^{(1),e} - \bar{w}_i^{(2),e}) d\Gamma_e \\ & \left. + \frac{(\int_{\Gamma_e} (\bar{w}_i^{(1),e} - \bar{w}_i^{(2),e}) d\Gamma_e \int_{\Gamma_e} (\bar{u}_k^{(1),e} - \bar{u}_k^{(2),e}) d\Gamma_e) [A_{ik}]^e}{\int_{\Gamma_e} (b^{(1),e} - b^{(2),e}) d\Gamma_e \int_{\Gamma_e} (b^{(1),e} - b^{(2),e}) d\Gamma_e} \right] = 0 \quad \text{for all } \mathbf{w} \in V \quad (63) \end{aligned}$$

where

$$A_{ik}^e = \sum_{m^e} \int_{v_e} \left( \frac{\partial b^e}{\partial x_j} \right)^{(m^e)} C_{ijkl}^{(m^e)} \left( \frac{\partial b^e}{\partial x_l} \right)^{(m^e)} dv_e \quad (64)$$

The script  $e$  indicates an element quantity, used here to index bulk elements. The last three terms on the left side will only contribute to elements  $e$  intersected by  $\Gamma_*$ . Thus,  $m^e$  is an index over the two grains (1 and 2) on either side of the interface  $\Gamma_*$ ,  $\Gamma_e$  is a subsegment of  $\Gamma_*$  interior to element  $e$ , and  $\langle \bar{\sigma}_{kl}(\bar{w}) \rangle^e$  is an element wise stress value.

Equations (24) (Nitsche) and (63) (bubble stabilization) are similar in many ways. The first two terms on the left side of (24) together correspond to the first term in (63). The third term on the left side of (24) is the stabilization term, analogous to the last term in (63). There is an appreciable

difference here, however, as  $\alpha$  from Nitsche's method becomes an element-wise matrix operator with a value dependent on the form of the element bubble:

$$\alpha_{ik}^e = \frac{[A_{ik}]^e}{\int_{\Gamma_e} (b^{(1),e} - b^{(2),e}) d\Gamma_e \int_{\Gamma_e} (b^{(1),e} - b^{(2),e}) d\Gamma_e} \quad (65)$$

where  $[A_{ik}]^e$  is given by (64).

As in the case of Nitsche's method, an approximation of the Lagrange multipliers can be extracted to build the traction field over the interface, via

$$\lambda_i^e = \left( \frac{[A_{ik}]^e}{\int_{\Gamma_e} (b^{(1),e} - b^{(2),e}) d\Gamma_e \int_{\Gamma_e} (b^{(1),e} - b^{(2),e}) d\Gamma_e} \right) \left( \int_{\Gamma_e} [\tilde{u}_k^e] d\Gamma_e \right) - \langle \sigma_{ij} \rangle^e n_j \quad (66)$$

The discrete form of the equations in the bubble-stabilized method are almost identical to Nitsche's method. The key implementational addition is the selection of bubble functions over the elements, and the calculation of  $\alpha$ , which is now a matrix operator and potentially different over every boundary segment  $\Gamma_e$ . We have chosen the product of the linear shape functions over the triangular domain as a suitable bubble function. The element-based stabilization  $\alpha$  is calculated via (65) and (64). We note that the quantity  $\alpha$  is now a matrix (number of spatial dimensions by number of spatial dimensions) owing to the  $A_{ik}$  in the numerator.  $A_{ik}$  is calculated in the entire element interior of the element containing a boundary segment, and the denominator of Equation (65) is calculated over the segment itself. In general, enrichment of the bubble elements follows the same rules as enrichment of coarse scale degrees of freedom, which is to say, elements cut by an edge of  $\Gamma_e$  will only be enriched with one characteristic function  $H$ . Thus, it can be expected that one of either  $b^{(1),e}$  or  $b^{(2),e}$  will be multiplied by 1 and the other by 0.

The stabilization contribution to the stiffness for an element is now formulated through

$$\mathbf{k}_e^s = \int_{\Gamma_e} \mathbf{N}^{eT} d\Gamma_e \boldsymbol{\alpha} \int_{\Gamma_e} \mathbf{N}^e d\Gamma_e \quad (67)$$

with an element-based matrix  $\boldsymbol{\alpha}$ :

$$\boldsymbol{\alpha} = [\alpha_{ik}^e]$$

All other stiffness terms are calculated as in Nitsche's implementation.

## 5. MULTIPLE GRAINS AND TRIPLE JUNCTIONS

It is equally possible to apply the previously described methods to domains comprised of more than two grains and one interface. Having more than two grains in the physical domain introduces the need to handle triple junctions. Figure 5 shows a plausible element configuration with three different grain domains in a single element. In an element where there is a triple junction, each segment is treated as a separate  $\Gamma_*$ . The contributing terms to the variation term for the constraint of that segment come from the portions of the element containing the grains on either side of the interface. It can be seen in the figure that though there is a global grain numbering scheme  $G^{(m)}$ , there will also be a local index,  $m$  or  $m^e$ , which only runs from 1 to 2. The complete stiffness contribution of an element such as in Figure 5 will come from three successive applications of

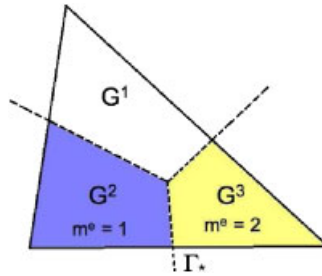


Figure 5. Example of a triple grain junction in an element.

the appropriate variational form, one for each separate interface segment. In each loop, the local index  $m$  will switch to two different grains. Such an implementation also allows different segments in a triple junction in a single element to be treated with different constraint types (for example, one interface would have a tied constraint while another could be allowed to separate). Additionally, for enriched nodes, we enrich with characteristic functions from one less than the amount of grains represented in the nodal support. Enriching with all of the grains and including the background degrees of freedom would result in linear dependencies. Thus, a node with supports crossed by an intersection would have degrees of freedom from the background field, as well as one or other of the grains on either side of the intersection, but not both [20].

## 6. NUMERICAL RESULTS

We now provide numerical results to several two-dimensional benchmark problems in elasticity, including a patch test, plane stress beam bending, and a thick-walled pressure vessel. Finally, we examine the elastic response of a domain consisting of multiple grains and triple junctions. When appropriate, results are compared with control cases without interfaces or to cases where interfaces are explicitly fitted to the mesh.

### 6.1. Patch test

We consider a simple variation on the standard linear patch test for elements (see [23]). A nine-node, 8 element ‘patch’ of non-degenerate elements is partitioned into two regions, or grains, by a single interface. Both grains are given the same material properties. A displacement is prescribed to all exterior nodes in four different fashions, corresponding to two pure tensile states of stress and two pure shear states of stress. The only unknown is the displacement at a center node, which only attains the correct value if the interface is properly constrained.

The Lagrange multiplier method, Nitsche’s method, and the bubble-stabilized method all pass the patch test to machine precision. With Nitsche’s method, the test is passed regardless of the choice of  $\alpha$ . The penalty method does not pass the patch test, which is expected as it is not variationally consistent. The error in the patch test for the penalty is a function of  $\alpha$ , and decreases as  $\alpha$  is increased.

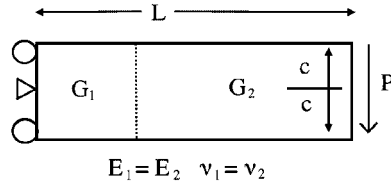


Figure 6. Geometry for beam bending test problem.

## 6.2. Beam bending

Consider a two-dimensional problem of elastic, linear isotropic plane stress beam bending. The setup and elastic solution are taken from [23, pp. 219–221]. A schematic of the domain and boundary conditions is given in Figure 6. The beam has height  $2c$ , length  $L$ , and unit depth. For a continuous beam (that is, without an interface) there is an exact elasticity solution that exists if the boundary conditions are carefully specified. At the left end, the displacement of the center node is completely fixed, via

$$u_1(0, 0) = u_2(0, 0) = 0.0 \quad (68)$$

The top and bottom left most nodes are constrained in the  $x$ -direction, via

$$u_1(0, \pm c) = 0.0 \quad (69)$$

A shear force with resultant  $P$  is distributed parabolically over the right end surface. At the left end, shear tractions are prescribed equal and opposite to those on the right end, and normal tractions are prescribed linearly (except on constrained nodes) in a such a way to balance the moments caused by the right end forcing. The top and bottom surfaces are traction-free. In equation form, the traction boundary conditions are given as

$$h_1(L, y) = 0 \quad (70)$$

$$h_2(L, y) = \frac{P}{2I}(c^2 - y^2) \quad (71)$$

$$h_1(0, y) = \frac{PLy}{I} \quad (72)$$

$$h_2(0, y) = -\frac{P}{2I}(c^2 - y^2) \quad (73)$$

where  $I$  is the area moment of inertia,  $I = (2c)^3/12$ .

The analytical solution for the displacement field is

$$u_1(x, y) = -\frac{Py}{6EI}[3(L^2 - \tilde{x}^2) + (2 + \nu)(y^2 - c^2)] \quad (74)$$

$$u_2(x, y) = -\frac{Py}{6EI}\{(\tilde{x}^3 - L^3) + [(4 + 5\nu)c^2 + 3L^2](\tilde{x} - L) + 3\nu\tilde{x}y^2\} \quad (75)$$

where  $\tilde{x} = L - x$ . The stresses are

$$\sigma_{xx} = -\frac{P\tilde{x}y}{I} \tag{76}$$

$$\sigma_{yy} = 0 \tag{77}$$

and

$$\sigma_{xy} = \frac{P}{2I}(c^2 - y^2) \tag{78}$$

For the numerical calculations, the following values were used:  $P = -1000$ ,  $L = 16$ ,  $c = 2$ ,  $E = 1000$ , and  $\nu = 0.3$ .

We performed calculations using a standard finite element mesh with and without a vertical interface inserted at  $x = 5$ . A tied intersection should approximate the solution with the same accuracy as a standard FE method. The domain was discretized first with a structured mesh, then with an unstructured mesh, and refined in a self similar way. Figures 7 and 8 show examples of typical structured and unstructured meshes.

In the case of both Nitsche’s method and penalty methods, it was necessary to specify the value of  $\alpha$ . In both cases, experimentation with values showed that there was an optimal range for accuracy, depending on the quantity of interest. For very low values of  $\alpha$  the stiffness matrix for Nitsche’s method is not positive definite, and the approximate field displayed non-physical oscillations. The penalty method displayed large errors for very low  $\alpha$ . For very large values of  $\alpha$ , both Nitsche’s method and the penalty method showed highly oscillatory behavior in the traction profiles over the interface. For Nitsche’s method, the lowest value of  $\alpha$  that yielded a positive definite stiffness matrix was used and appeared to also be optimal in terms of accuracy in the  $L^2$  norm of the error. The value can be estimated for each mesh using Equation (51). For the mesh shown in Figure 7, and the given material parameters,  $\alpha$  was found to be 9000 for Nitsche. The best value for  $\alpha$  (based on the  $L^2$  norm) was determined empirically for the penalty method for each mesh, and was seen to scale as  $1/h$ . The results that are given thus represent the best possible case for the penalty method results. It bears emphasis that this approach is not available for most problems, and is only employed in this case for illustrative purposes.

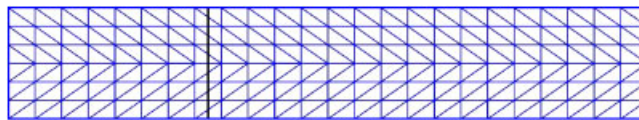


Figure 7. A typical structured mesh for the beam bending test problem.

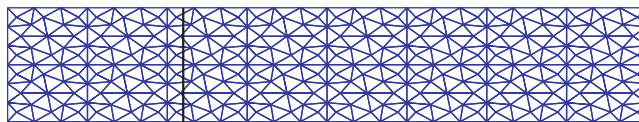


Figure 8. A typical unstructured mesh for the beam bending test problem.

The  $L^2$  norm of the errors in the bulk displacement field is expected to show quadratic convergence. From Figure 9, it is apparent that most of the methods enforce the tied constraint well enough to maintain optimal convergence in the bulk field norms. There is some lack of uniformity in the rate for the penalty method results, which are especially sensitive to the penalty parameter. Overall, it is difficult to differentiate the methods based solely on the error in the displacement field.

By contrast, the accuracy of the traction field over the interface shows much more variation among the methods. For the beam bending problem with a vertical interface, the traction component  $t_x$  is representative of the bending stresses, and takes a linear profile over the height of the interface. The component  $t_y$  is representative of the shear stresses and takes a parabolic profile in the same form as the right end loading. The approximate traction is extracted using (22) for the penalty method, (42) for Nitsche’s method, and (66) for the bubble-stabilized method. Figures 10, 11, 12,

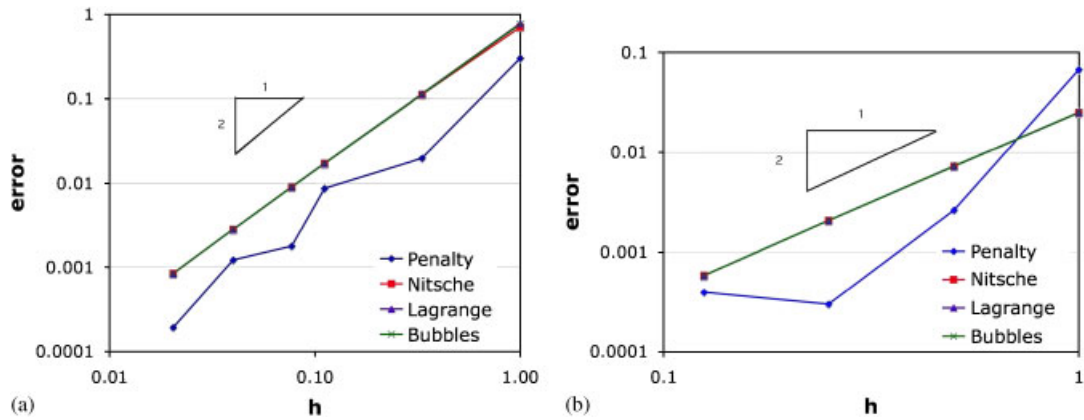


Figure 9. Spatial convergence in the  $L^2$  norm of displacement for beam bending problem using: (a) structured and (b) unstructured meshes.

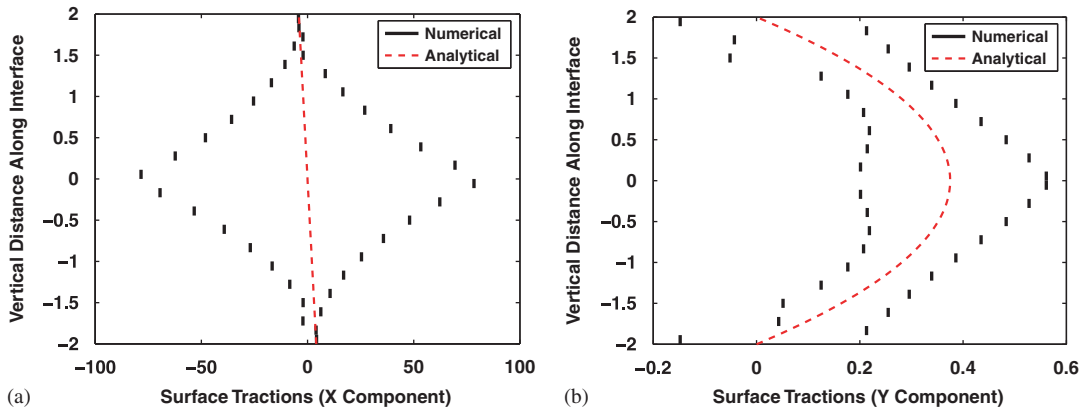


Figure 10. Interface traction for the Lagrange multiplier method (beam bending, structured mesh).

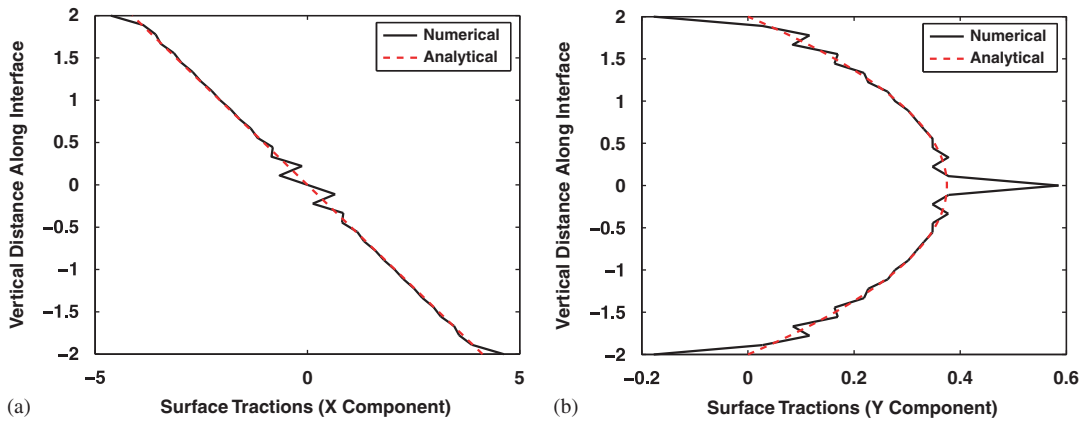


Figure 11. Interface traction for the penalty method (beam bending, structured mesh).

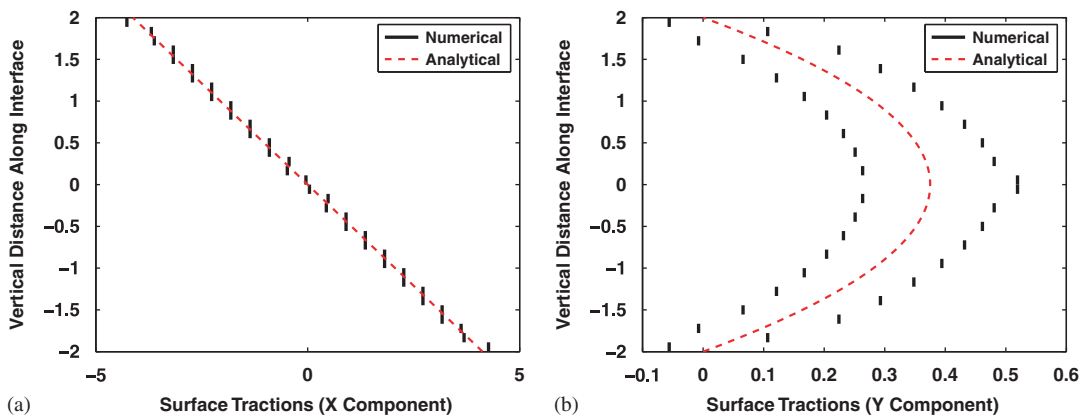


Figure 12. Interface traction for Nitsche's method (beam bending, structured mesh).

and 13 show the traction profiles along the interface for a mesh with 40 elements through the thickness of the beam.

The traction field with Lagrange multipliers is obviously unstable. Nitsche's method and the bubble-stabilized method also display an oscillatory pattern around the exact solution, but only in the shear field. The oscillations in this case are transmitted by shear locking in the linear triangles, which can be seen in a beam bending calculation performed with a standard conforming finite element formulation using constant strain triangles. The oscillations are spatially regular and the error is observed to decrease with mesh refinement. The penalty method produces a field that also exhibits large oscillations around key points.

Quantitatively, we can track the accuracy of the tractions by calculating the  $L^2$  norm of the traction error over the boundary. Optimal spatial convergence in this case occurs at a linear rate. It can be seen from Figure 14 that Nitsche's method and the bubble-stabilized method are the only

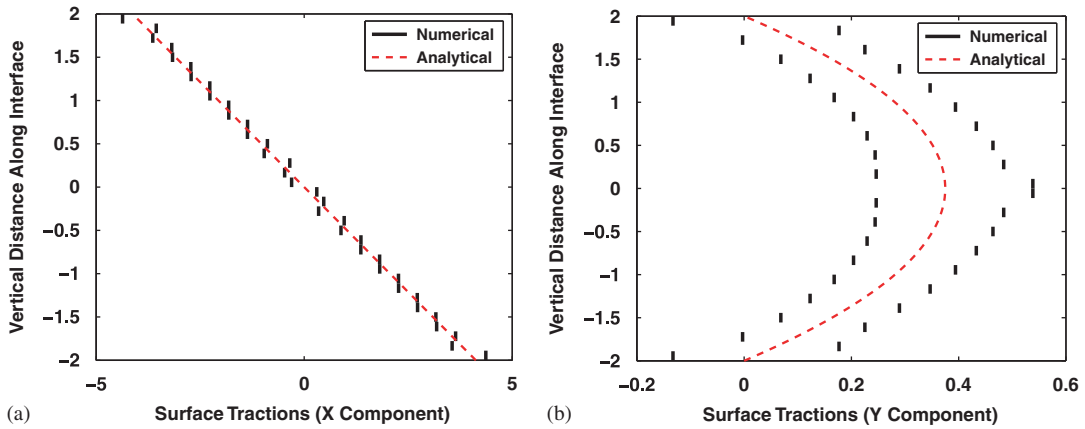


Figure 13. Interface traction for bubble-stabilized method (beam bending, structured mesh).

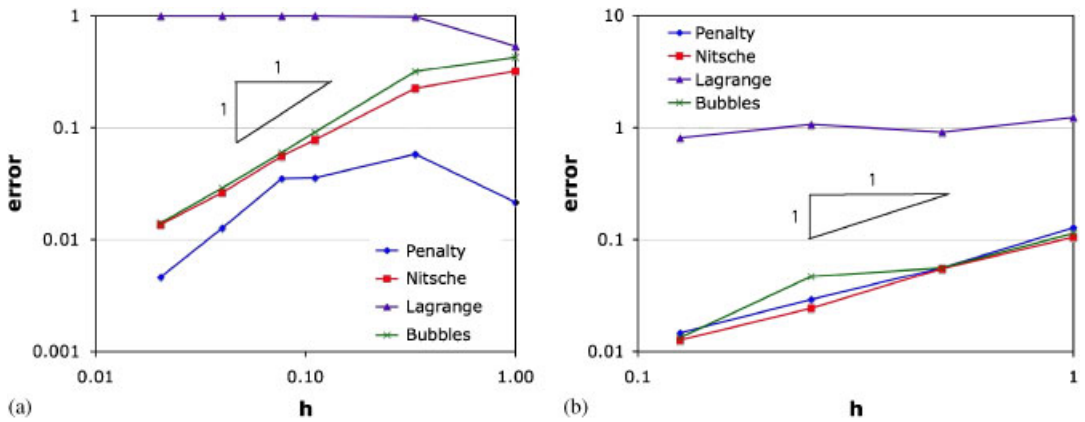


Figure 14. Spatial convergence of interface tractions in the  $L^2$  norm for beam bending for: (a) structured and (b) unstructured meshes.

techniques that exhibit good convergence. The traction field obtained using Lagrange multipliers does not converge. The penalty method does show a reduction in error with mesh refinement, but not in a monotonic way, and the results vary wildly depending on the value of the penalty parameter.

### 6.3. Pressure vessel

Consider the two-dimensional elasticity problem of a thick-walled cylindrical vessel with inner radius  $a$  and outer radius  $b$  (Figure 15), subject to a uniform pressure  $p$  on the interior surface. We assume that the outer surface is traction-free, and that plane stress conditions prevail. We only mesh a quarter of the problem domain and apply symmetry conditions on the appropriate boundaries. An

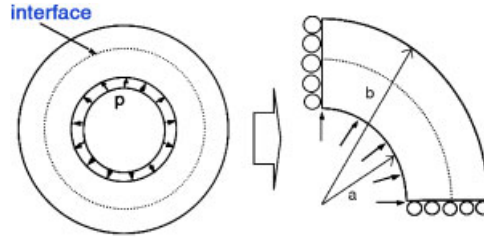


Figure 15. Setup for pressure vessel problem.

interface is inserted at a constant radius. In polar coordinates, the boundary conditions are

$$u_{\theta}(r, \theta = \pi/2) = 0 \quad (79)$$

$$u_{\theta}(r, \theta = 0) = 0 \quad (80)$$

$$h_r(r = a, \theta) = p \quad (81)$$

and

$$h_r(r = b, \theta) = 0 \quad (82)$$

Results reported here correspond to the case:  $a = 2$ ,  $b = 3$ ,  $E = 1000$ , and  $\nu = 0.0$ . The interface is placed at a radius of 2.5.

In polar coordinates, the exact displacement field is

$$u_{\theta} = 0 \quad (83)$$

and

$$u_r = \frac{(1 + \nu)a^2 p}{E(b^2 - a^2)} \left[ \frac{(1 - 2\nu)r}{1 + \nu} + \frac{b^2}{r} \right] \quad (84)$$

The corresponding stresses are

$$\sigma_r = \frac{pa^2(r^2 - b^2)}{r^2(b^2 - a^2)} \quad (85)$$

and

$$\sigma_{\theta} = \frac{pa^2(r^2 + b^2)}{r^2(b^2 - a^2)} \quad (86)$$

The problem is complicated by the fact that the interface is now curved, but simplified by the constant analytical solution for the traction field along the interface.

As with the beam bending problem, the methods are not differentiated by the errors in the approximate displacement fields. The convergence rate for all methods in the  $L^2$  norm is quadratic and the convergence of the traction fields at the interface shows a similar pattern as beam bending (Figure 16). The Lagrange multiplier method does not converge and the bubble-stabilized and Nitsche's method results converge at a better rate than those of the penalty method. Though the

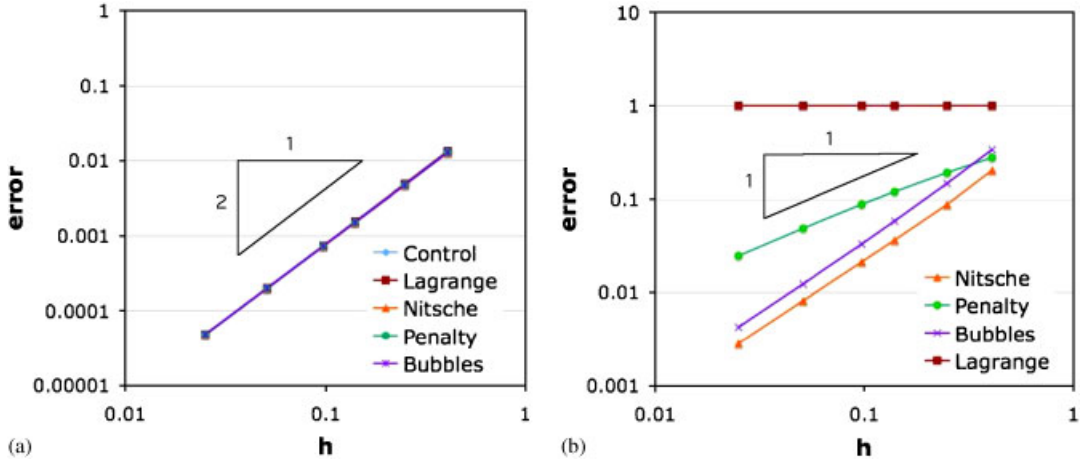


Figure 16. Spatial convergence of: (a) displacements and (b) interface tractions in the  $L^2$  norm (pressure vessel problem).

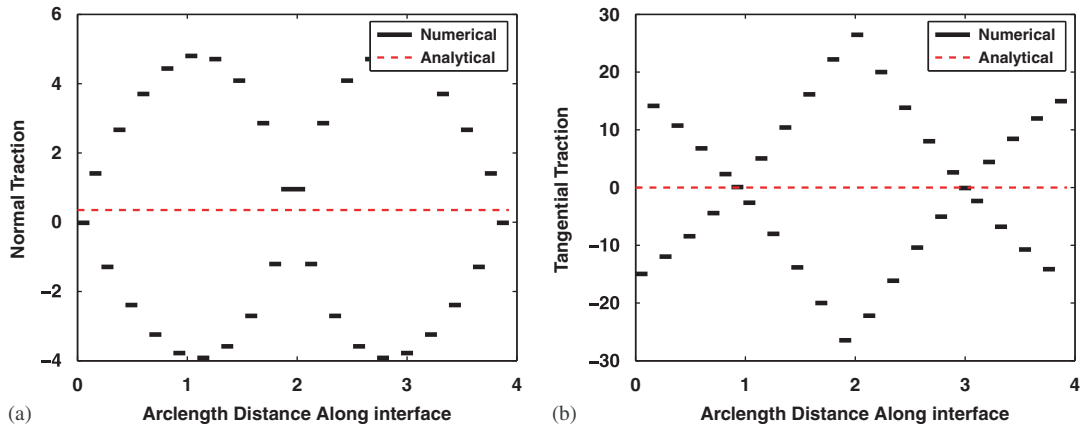


Figure 17. Interface traction for the Lagrange multiplier method (pressure vessel).

bubble-stabilized and Nitsche’s method results converge at the same rate, in this case it appears that the eigenvalue problem for Nitsche’s method produced a better value for  $\alpha$  for each mesh. Values for  $\alpha$  were chosen using the same method described in Section 6.2. The value for  $\alpha$  given by the bubble-stabilized method depends not only on the shape of the bubble function, but also on the location of the interface in the element interiors. Though the choice of  $\alpha$  given by the method appears to always be optimal in the sense of spatial convergence, it is not entirely unexpected that there may be slightly better choices available for a given mesh. Examples of the traction distribution for each method are given in Figures 17, 18, 19, and 20.

An aspect of the enriched finite element method is that it admits different material properties within different granular regions. The efficacy of the approach was demonstrated by reexamining

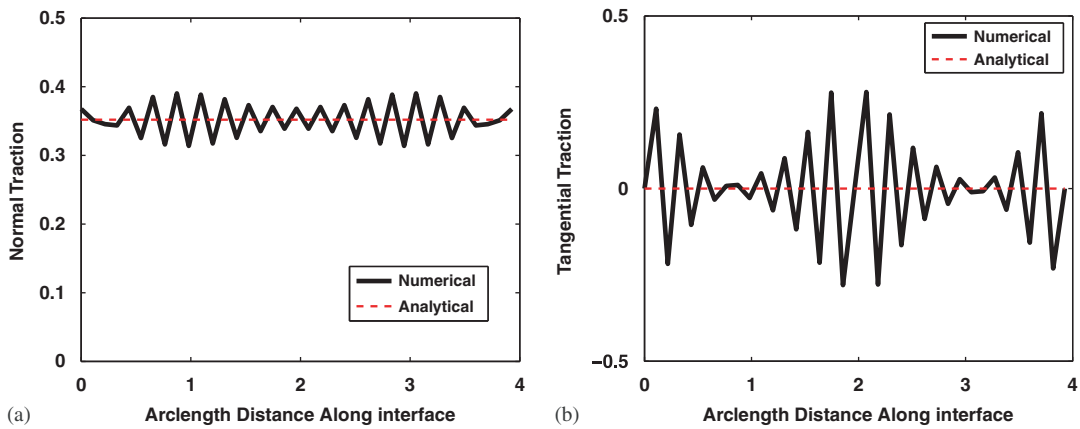


Figure 18. Interface traction for the penalty method (pressure vessel).

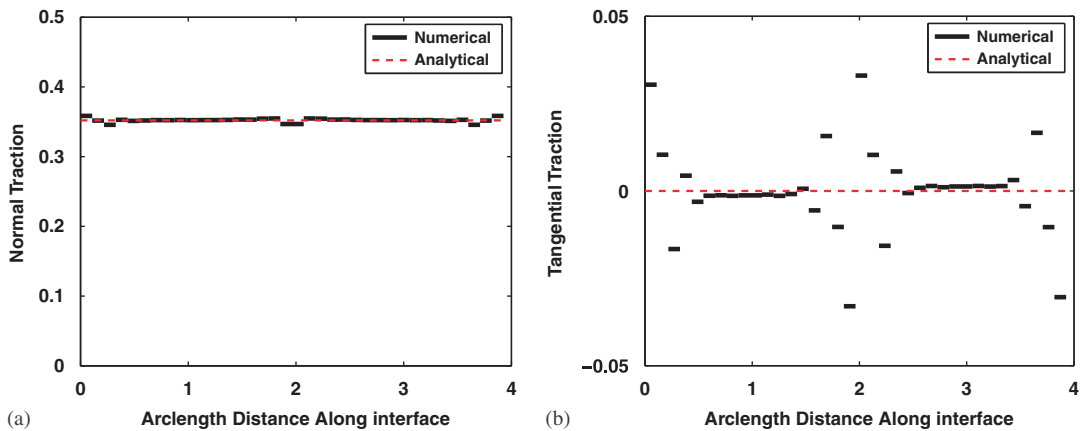


Figure 19. Interface traction for Nitsche's method (pressure vessel).

the pressure vessel problem with a bimaterial interface. The outer material was given Young's modulus of twice the inner material. Figure 21 shows the convergence results for the traction field over the interface in this case.

#### 6.4. Multiple grain elasticity

Figure 22 represents a body with multiple grains and triple junctions. The geometry represents a symmetric and regular grain pattern that has been seeded with small random geometric perturbations. There are 23 grains, each with slightly different material properties. The elastic moduli of the grains was given a Gaussian distribution with a mean of  $3 \times 10^7$  and a variance of  $6 \times 10^6$ , while  $\nu=0$  for all of the grains. When fixed at one end, and with a uniform pressure applied

STABILIZING CONSTRAINTS OVER ENRICHED INTERFACES

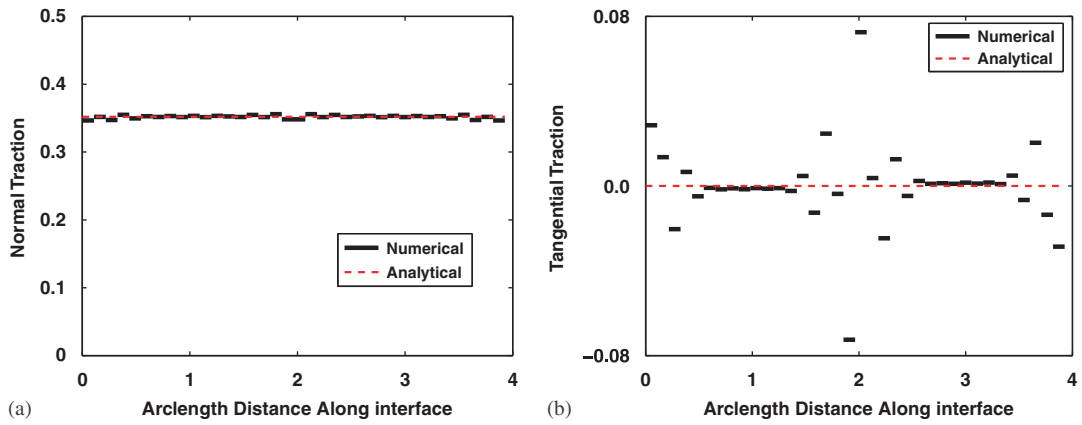


Figure 20. Interface traction for the bubble-stabilized method (pressure vessel).

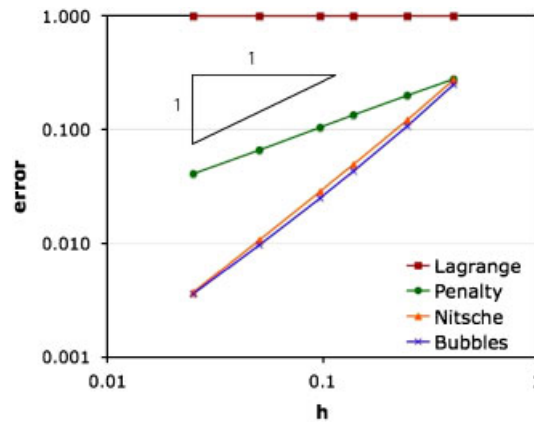


Figure 21. Spatial convergence of interface tractions in the  $L^2$  norm (bimaterial pressure vessel problem).

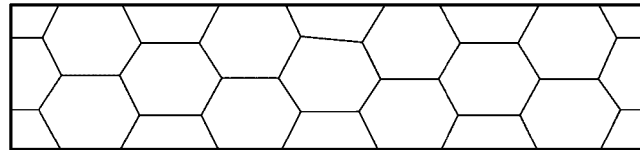


Figure 22. Physical domain and grain boundaries for an elasticity problem with multiple grains.

at the other, the overall end displacement is similar to what would occur if all of the grains were given a material property of  $3 \times 10^7$ , but there are local variations in the internal stresses. Figures 23 and 24 show contours of the internal stresses,  $\sigma_{xx}$  for a standard mesh in which the

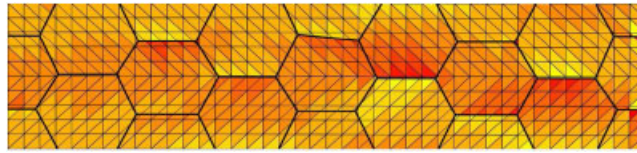


Figure 23.  $\sigma_{xx}$  for an enriched mesh over multiple grains.

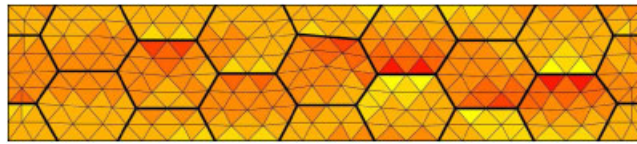


Figure 24.  $\sigma_{xx}$  for a conformal mesh over multiple grains.

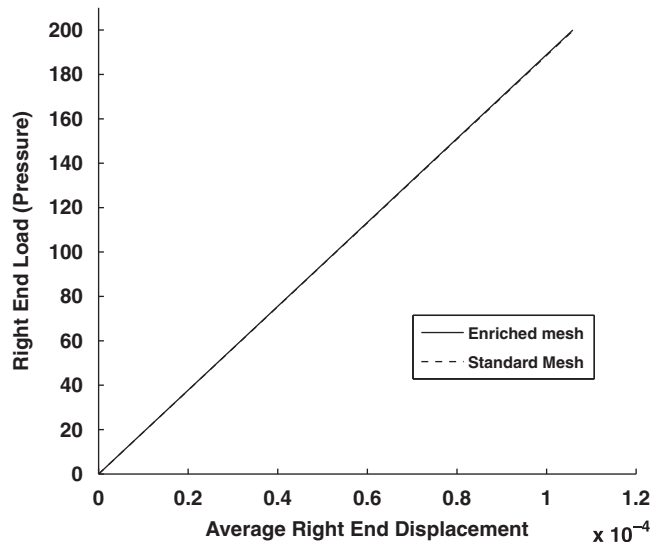


Figure 25. The pressure-end displacement relationship predicted for the multi-grain example.

grains are explicitly gridded, and an enriched mesh with tied interfaces. Within the precision of the contouring, the results are the same for Nitsche's method and the bubble-stabilized method. The contours represent stresses ranging from 160 (lightest) to 240 (darkest). In the traditional mesh, the body is continuously connected. It is apparent that the results are similar for a traditional finite element mesh and an enriched mesh. In addition, we can see from Figure 25 that there is no appreciable change in overall stiffness between the two meshes.

## 7. CONCLUSIONS

While a great deal of research concerned with enriched finite element methods has focused on capturing internal discontinuities, fairly little attention has focused on the important problem of enforcing internal constraints. In the case of X-FEM, discontinuous enrichment of finite element basis functions allows the construction of a solution space that takes into account discontinuities at grain boundaries in a polycrystalline topography without the disadvantage of needing to grid the interfaces. The introduction of the discontinuity should ultimately facilitate the modeling of appropriate grain boundary behavior at the interfaces. To investigate the numerics of imposing constraints along these discontinuities, in this work we examined the strictest possible constraint of continuity. While such a constraint appears counterintuitive with discontinuous enrichment functions, the latter nonetheless provide a means to capture slope discontinuities across material interfaces.

Previous work had shown that penalty methods can be unreliable for our particular formulation, a result which our studies confirm. Other major disadvantages of the penalty method include the tendency toward ill-conditioning and the sensitivity of the method to the penalty parameter. It appears that our interpolation of Lagrange multipliers is unable to satisfy the LBB, or ‘inf-sup’ stability conditions. A key point in the interpolation of the Lagrange multipliers is that the modeler has very little control over how and where the multipliers are interpolated. The basis for the multipliers is determined by the intersection of the interface with the background mesh. Lagrange multipliers, then, are almost always unstable for embedded interface problems.

Based on previous work, we anticipated that Nitsche’s method would be a stable and convergent method to impose tied constraints. All of our numerical examples show optimal rates of convergence in the interfacial traction for Nitsche’s method. Although some small oscillations were observed in some problems in the traction field, these oscillations were also observed in conforming finite element treatments of the same problems—meaning that the Nitsche version of the enriched method provided results at least as good as those produced by a standard finite element method using the same elements in a conforming configuration. Furthermore, it is possible that a weighted smoothing method could be applied to the traction field. Such a weighting method was successfully applied in the work by Mourad *et al.* [18] and Ji and Dolbow [7] but nothing has yet been investigated in the context of elasticity problems.

A future improvement of the method might involve a better system to choose the form of the bubble functions, which essentially govern the local values of the stabilization parameter  $\alpha$ . In addition, this work only demonstrated the enforcement of constraints in the context of static linear elasticity. For realistic simulations of many processes of interest for polycrystalline materials, it would be necessary to investigate the method within the context of dynamics, finite deformation kinematics and plasticity. Additionally, there are other possible directions to which the idea of un-gridded intersections may be applied, perhaps even the coupling of multi-physics problems or combining Eulerian and Lagrangian grids.

## ACKNOWLEDGEMENTS

The authors would like to acknowledge the support of the Air Force Office of Scientific Research Grant FA9550-06-1-0108, the Department of Defense National Defense Science and Engineering Fellowship Program, the Department of Energy, and Sandia National Laboratories.

REFERENCES

1. Moës N, Dolbow J, Belytschko T. A finite element method for crack growth without remeshing. *International Journal for Numerical Methods in Engineering* 1999; **46**:131–150.
2. Duarte CA, Babuška I, Oden JT. Generalized finite element methods for three dimensional structural mechanics problems. *Computers and Structures* 2000; **77**:215–232.
3. Belytschko T, Moës N, Usui S *et al.* Arbitrary discontinuities in finite elements. *International Journal for Numerical Methods in Engineering* 2001; **50**:993–1013.
4. Simone A. Partition of unity-based discontinuous elements for interface phenomena: computational issues. *Communications in Numerical Methods in Engineering* 2004; **20**:465–478.
5. Moës N, Béchet E, Tourbier M. Imposing Dirichlet boundary conditions in the extended finite element method. *International Journal for Numerical Methods in Engineering* 2006; **67**:1641–1669.
6. Geniaut S, Massin P, Moës N. A stable 3D contact formulation using X-FEM. *REMNUM*, 2006.
7. Ji H, Dolbow J. On strategies for enforcing interfacial constraints and evaluating jump conditions with the extended finite element method. *International Journal for Numerical Methods in Engineering* 2004; **61**:2508–2535.
8. Farhat C, Harari I, Franca L. The discontinuous enrichment method. *Computer Methods in Applied Mechanics and Engineering* 2001; **190**:6455–6479.
9. Gracie R, Wang H, Belytschko T. Blending in the extended finite element method by discontinuous Galerkin and assumed strain methods. *International Journal for Numerical Methods in Engineering* 2008; **74**:1645–1669.
10. Lew A, Boscaglia G. A discontinuous-Galerkin-based immersed boundary method. *International Journal for Numerical Methods in Engineering* 2008; **76**:427–600.
11. Wang H, Belytschko T. Fluid-structure interaction by the discontinuous-Galerkin method for large deformations. *International Journal for Numerical Methods in Engineering* 2008; DOI: 10.1002/nme.2396.
12. Nitsche J. Über ein Variationsprinzip zur Lösung von Dirichlet-Problemen bei Verwendung von Teilräumen, die keinen Randbedingungen unterworfen sind. *Computer Methods in Applied Mechanics and Engineering* 1971; **191**:1895–1908.
13. Stenberg R. On some techniques for approximating boundary conditions in the finite element method. *Journal of Computational and Applied Mathematics* 1995; **63**:139–148.
14. Barbosa JC, Hughes TRJ. The finite element method with Lagrange multipliers on the boundary: circumventing the Babuška–Brezzi condition. *Computer Methods in Applied Mechanics and Engineering* 1991; **85**:109–128.
15. Griebel M, Schweitzer MA. A particle-partition of unity method part V: boundary conditions. *Geometric Analysis and Nonlinear Partial Differential Equations* 2002; **41**:115–137.
16. Fernández-Méndez S, Huerta A. Imposing essential boundary conditions in mesh-free methods. *Communications in Numerical Methods in Engineering* 2004; **193**:1257–1275.
17. Hansbo A, Hansbo P, Larson MG. A finite element method on composite grids based on Nitsche’s method. *Mathematical Modeling and Numerical Analysis* 2004; **37**:47–51.
18. Mourad H, Dolbow JE, Harari I. A bubble-stabilized finite element method for Dirichlet constraints on embedded interfaces. *International Journal for Numerical Methods in Engineering* 2007; **69**:772–793.
19. Hughes TJR *et al.* The variational multiscale method—a paradigm for computational mechanics. *Computer Methods in Applied Mechanics and Engineering* 1998; **166**:3–24.
20. Simone A, Duarte CA, Van der Giessen E. Generalized finite element method for polycrystals with discontinuous grain boundaries. *International Journal for Numerical Methods in Engineering* 2006; **67**:1122–1145.
21. Babuška I. The finite element method with penalty. *Mathematics of Computation* 1973; **27**:221–228.
22. Dolbow J, Moës N, Belytschko T. Discontinuous enrichment in finite elements with a partition of unity method. *Finite Element Methods in Analysis and Design* 2000; **36**:235–260.
23. Hughes TRJ. *The Finite Element Method, Linear Static and Dynamic Finite Element Analysis*. Dover: New York, 2000.